DOI: 10.1002/ange.201210359

Optofluidics

A Plasmon-Assisted Optofluidic (PAOF) System for Measuring the Photothermal Conversion Efficiencies of Gold Nanostructures and Controlling an Electrical Switch**

*Jie Zeng, David Goldfeld, and Younan Xia**

In localized surface plasmon resonance (LSPR), the electrons in the conduction band of a plasmonic nanostructure are polarized by the alternating electric field of an incident light to collectively oscillate at a resonant frequency.[1,2] As a result, the incident light is absorbed by the plasmonic nanostructure. Some of the absorbed energy is emitted as light through scattering while the rest is dissipated by Landau damping,[3] resulting in light-to-heat conversion. Photothermal conversion has been used to induce localized heating of a host medium,[4] which is of great interest for applications in a number of fields, including photonics,[5] electronics,[6] catalysis,[7] phase transformation,[8] and biomedicine.[9]

Photothermal heating based on plasmonic nanostructures has also been explored as a means to induce and/or control fluid motion.[10] Lee and co-workers were able to mobilize liquid to move along microfluidic channels over a distance as far as 500 μm by using plasmonic heating with Au colloids.[11] In this case, the liquid was forced to move through a complex mechanism that involved a combination of localized evaporation, condensation, and surface wetting. Recently, Wu and co-workers were able to control liquid flow through microfluidic channels by combining the temperature-dependent sol–gel transformation with a composite of Au nanorods and poly(dimethyl siloxane) to generate localized obstructions within specific paths.[12] Most recently, Halas and co-workers exploited the localized heating of SiO_2/Au nanoshells within a solution to vaporize water and ethanol with sunlight.[13] They suggested that the nanoshells heated up rapidly upon irradiation, thus surrounding their surfaces by thin layers of high-temperature vapor that carried the nanoshells to the top of the suspension before the vapor was released into the atmosphere above.

Despite these reports, we noticed that the absorption cross sections of the plasmonic nanostructures, a fundamental property that determines their photothermal conversion efficiencies, were seldom measured experimentally in these studies. A quantitative understanding of this parameter is essential for the engineering of plasmonic nanostructures for a variety of applications, such as fluid transport, optical imaging contrast enhancement, and cancer treatment. In a prior study, we demonstrated the use of photoacoustic imaging for experimental measurements of the absorption cross sections of Au nanostructures, but this approach requires expensive equipment and complex procedures.[14]

Herein, we report a plasmon-assisted optofluidic (PAOF) system that consists of a diode laser as the energy source, an aqueous suspension of Au nanostructures as the photo-responsive fluidic medium, and a capillary as the means to monitor the change in temperature caused by volumetric expansion of the medium. Three different types of Au nanostructures were compared in this study: nanocages, nanorods, and hexapods; all of them can be tuned to absorb light in the near-infrared region. To achieve controllable fluid motion, we took advantage of the well-known thermal expansion phenomena of a liquid. With this system, we could cause a fluid to rise in a capillary by as much as 30 mm, depending on the type of nanostructures suspended in the medium and/or their concentration. We could also experimentally measure the absorption cross sections and photothermal conversion efficiencies of various types of plasmonic nanostructures. Furthermore, we demonstrated the feasibility of utilizing the fluid motion caused by plasmonic heating to construct a photo-sensitive electrical switch.

The PAOF system (Figure 1a) contained a diode laser with a central output wavelength of 808 nm, a photo-responsive medium, and a microfluidic device (Figure 1b). The microfluidic device was assembled from a poly(dimethyl siloxane) (PDMS) block (**1**) with a flat surface, a PDMS block patterned with a reservoir (**2**) on the surface, a plastic tube with an inner diameter of 0.5 mm (**3**) serving as a channel for pumping in the liquid medium, and a glass capillary with an inner diameter of 0.6 mm (**4**) serving as a "ruler" to measure volumetric expansion of the liquid. All joints were sealed with PDMS. The exact dimensions of these components are

[*] Dr. J. Zeng,[§] D. Goldfeld, Prof. Y. Xia[+]
Department of Biomedical Engineering
Washington University in St. Louis
Saint Louis, MO 63130 (USA)

[+] Current address: The Wallace H. Coulter Department of Biomedical Engineering, School of Chemistry and Biochemistry
School of Chemical and Biomolecular Engineering
Georgia Institute of Technology
Atlanta, Georgia 30332 (USA)
E-mail: younan.xia@bme.gatech.edu

[§] Current address: Hefei National Laboratory for Physical Sciences at the Microscale and Department of Chemical Physics
University of Science and Technology of China
Hefei 230026, Anhui (P.R. China)

[**] This work was supported in part by a research grant from NCI (1R01 CA138527), an NIH Director's Pioneer Award (DP1, OD000798), and startup funds from Washington University in St. Louis and Georgia Institute of Technology. Y.X. was also partially supported by the World Class University (WCU) program through the National Research Foundation of Korea, funded by the Ministry of Education, Science and Technology (R32-20031).

Supporting information for this article is available on the WWW under http://dx.doi.org/10.1002/anie.201210359.

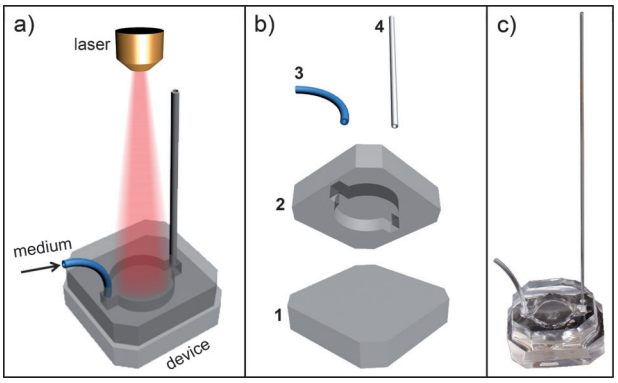

Figure 1. a) Plasmon-assisted optofluidic system. The arrow indicates the end of the plastic tube where the medium is pumped into the microfluidic device. b) Microfluidic device. **1**: PDMS block used to seal the reservoir. **2**: PDMS block cast with a reservoir to host the medium. **3**: Plastic tube that serves as a channel for pumping the medium. **4**: Glass capillary that is used to measure the volumetric expansion. c) Photograph of an assembled optofluidic system.

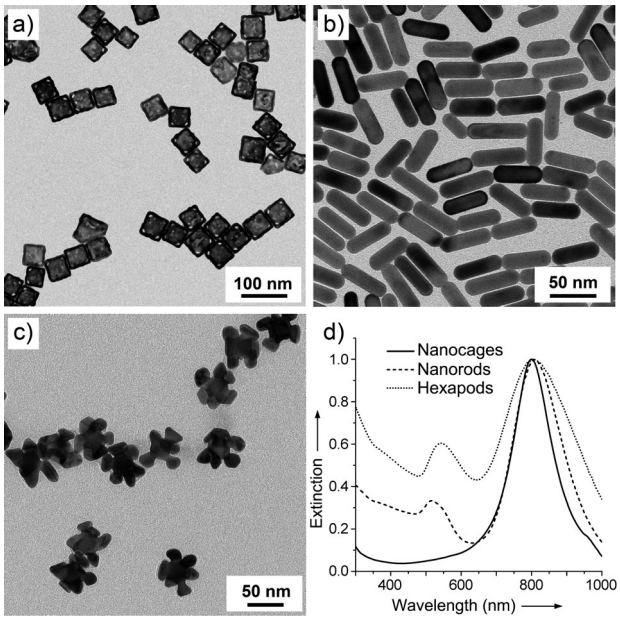

Figure 2. TEM images of the three types of Au plasmonic nanostructures used for converting light into heat: a) nanocages, b) nanorods, and c) hexapods. d) UV/Vis/NIR extinction spectra of the three different types of Au nanostructures.

summarized in Figure S1 in the Supporting Information. In a typical experiment, 0.7 mL of a medium containing the plasmonic nanostructures was loaded through the plastic tube into the reservoir between blocks **1** and **2** until the medium reached a height of 1 cm in the capillary. The opening on tube **3** was then plugged with a short glass rod. Since PDMS is transparent in the visible and near-infrared regions, the diode laser was able to penetrate through the top PDMS block to reach the liquid medium containing the plasmonic nanostructures. As such, the medium was quickly heated to a temperature as high as 84 °C, depending on the type of nanostructures contained in the medium and their concentration. The medium then thermally expanded into capillary **4** as a result of the increase in temperature, and the height of the liquid column was recorded with a stationary camera during irradiation. Figure 1c shows a photograph of the actual microfluidic device.

In the initial study, we compared the performance of three different types of Au plasmonic nanostructures: nanocages, nanorods, and hexapods. All of them can be engineered to generate heat through absorption of near-infrared light. The detailed procedures for the syntheses of these nanostructures can be found in the Supporting Information. Figure 2a–c shows transmission electron microscopy (TEM) images of these nanostructures. The nanocages (Figure 2a) exhibited a porous morphology (with a hollow interior and pores at the corner sites) with an outer edge length of 45 nm and a wall thickness of around 5 nm.[15] The nanorods (Figure 2b) had an average diameter of 17 nm and an aspect ratio of about 3.3.[16] The hexapods (Figure 2c) showed a highly branched morphology featuring an octahedral core with an edge length of approximately 25 nm and six arms on all the vertices.[17] The average distance between the ends of two opposite vertices was around 60 nm. In principle, the LSPR peaks of all these nanostructures can be precisely tuned to any wavelength in the near-infrared region by adjusting their wall thickness, aspect ratio, and arm length, respectively. In this study, all major LSPR peaks were tuned to the region of 805–810 nm to match the central output wavelength (808 nm) of the diode laser. Figure 2d shows UV/Vis/NIR extinction spectra of these three different types of Au nanostructures.

We used an organic dye, indocyanine green (ICG), as a reference of calibration. To establish a relationship between the temperature and the height of the liquid in the capillary, we calibrated the PAOF system by adding an aqueous solution of ICG (6.5 μM, 0.7 mL) to the device, irradiating the medium with the diode laser, monitoring the temperature (T) of the medium in real time with an infrared camera, and recording the height (h) of the medium in capillary **4** whenever the temperature reached 24, 37, 50, and 70 °C. The power density of the laser was set to 0.4 $W \cdot cm^{-2}$ and the illumination area was 1.13 cm^2 for all the experiments. A linear relationship was found between h and T (see Figure S2 in the Supporting Information). The slope ($\Delta h/\Delta T$) was calculated to be 0.52 mm $°C^{-1}$. Since all the media we used were based on aqueous solutions and should thus have more or less the same volumetric expansion coefficient, it is not unreasonable to assume that the calibration value for $\Delta h/\Delta T$ can also be applied to media that contain different types of Au nanostructures. The linear relationship between h and T suggests that the temperature of a medium can be determined by simply measuring the height (h) of the liquid in the capillary, just like with a thermometer.

We then evaluated the plasmon-assisted heating process over a period of 40 min. The diode laser was turned on for 10 min to heat the medium, and then turned off for 30 min to let the medium cool down. This process was repeated three times and the height was recorded at an interval of 1 min. For nanocages, we carried out measurements at four different concentrations (1.0×10^9, 2.5×10^9, 5.0×10^9, and 1.0×10^{10} particles/mL; Figure 3a), while for both nanorods and

hexapods, we only examined one concentration (1.0×10^{10} particles/mL; Figure S3). The curves clearly show the periodicity of change in height (Δh). As expected, the Δh value increased with the concentration of the nanostructures as a result of the increased absorption ability of the solution. For nanocages at a concentration of 1.0×10^{10} particles/mL, we were able to force the fluid up to a height of around 30.5 mm in the capillary. We then calculated the change in temperature (ΔT) based on the calibration value for $\Delta h/\Delta T$ (Table 1). For nanocages at different concentrations, ΔT varied from around 11.2 to around 58.7 °C, which corresponded to a maximum temperature of 82.7 °C when we started from room temperature (24 °C). For nanorods and hexapods, the ΔT values were less than half of that for nanocages at the same particle concentration.

To quantitatively evaluate the capability of converting light into heat for different types of plasmonic nanostructures, we calculated the energy conversion efficiency (η) using the following equation:

$$\eta = Q/E \tag{1}$$

where Q, which is the total heat generated in the solution, depends on ΔT at a given particle concentration, and E is the total energy output of the laser over a period of 10 min (see also Supporting Information). Table 1 summarizes Δh, ΔT, and η for nanocages, nanorods, and hexapods at various concentrations. As the concentration of nanocages increased from 1.0×10^9 to 2.5×10^9, 5.0×10^9, and 1.0×10^{10} particles/mL, η increased from $12.1\pm0.8\%$ to $27.9\pm1.7\%$, $46.9\pm2.9\%$, and $63.6\pm4.2\%$, respectively (see Table 1 and Figure 3b). For nanorods and hexapods at a concentration of 1.0×10^{10} particles/mL, the η values were $22.1\pm1.7\%$ and $29.6\pm1.9\%$, respectively, which were less than half of that for nanocages at the same concentration. The disparity in η for the three types of nanostructures is believed to be caused by their differences in absorption coefficient (μ) associated with absorption cross section (σ), an intrinsic property of the plasmonic nanostructure that determines its ability to absorb light at a particular wavelength.

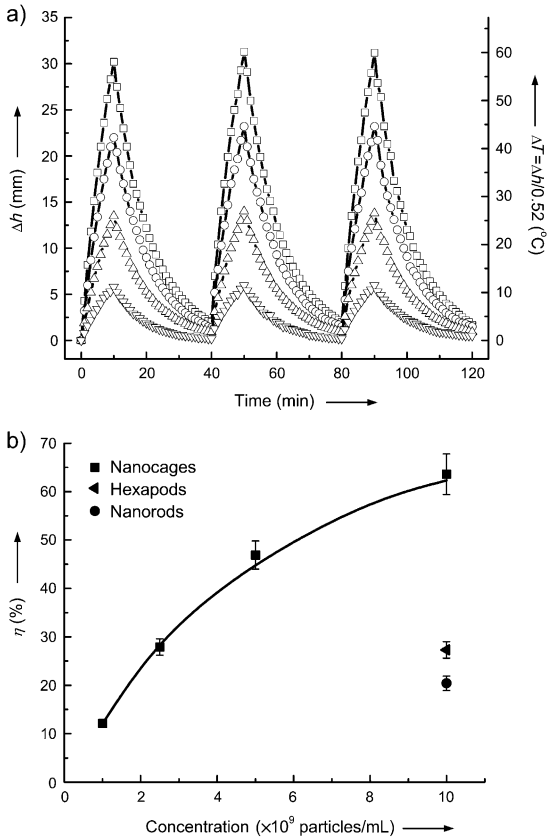

Figure 3. a) Plot of the rise in height (Δh) and increase in temperature (ΔT) upon irradiation as a function of time with suspensions of Au nanocages at four different concentrations: 1.0×10^9 (▽), 2.5×10^9 (△), 5.0×10^9 (○), and 1.0×10^{10} (□) particles/mL (from bottom to top). Each cycle of irradiation lasted for 40 min (irradiation on for 10 min and then off for 30 min) and the cycle was repeated three times. b) Plot of the energy conversion efficiency (η) as a function of particle concentration. For all irradiation processes, the laser density was set to 0.4 $W cm^{-2}$ and the illuminated area was 1.13 cm^2.

Table 1: Comparisons of the rise in height (Δh), increase in temperature (ΔT), energy conversion efficiency (η), absorption coefficient (μ), and absorption cross section (σ) for Au nanocages, nanorods, and hexapods at different particle concentrations. For each measurement, the sample was irradiated for 10 min.

	Nanocages				Nanorods	Hexapods
Concentration (particles/mL)	1.0×10^9	2.5×10^9	5.0×10^9	1.0×10^{10}	1.0×10^{10}	1.0×10^{10}
Δh [mm]	5.8 ± 0.4	13.4 ± 0.8	22.5 ± 1.4	30.5 ± 2.0	10.6 ± 0.8	14.2 ± 0.9
ΔT [K]	11.2 ± 0.8	25.8 ± 1.5	43.3 ± 2.7	58.7 ± 3.8	20.4 ± 1.5	27.3 ± 1.7
η [%]	12.1 ± 0.8	27.9 ± 1.7	46.9 ± 2.9	63.6 ± 4.2	22.1 ± 1.7	29.6 ± 1.9
μ [m^{-1}]	18.4 ± 1.3	45.4 ± 3.1	83.5 ± 6.5	123.6 ± 11.6	35.0 ± 3.0	48.5 ± 3.5
σ [$\times10^{-15}$ m^2]	18.4 ± 1.3	18.2 ± 1.2	16.7 ± 1.3	12.4 ± 1.2	3.5 ± 0.3	4.9 ± 0.4

One of the major applications of the PAOF system is to experimentally measure the μ and thus calculate the σ of a plasmonic nanostructure. To demonstrate this capability, we used ICG as a reference, again because its absorption coefficient (μ_{ICG}, which equals 140 m^{-1}) is well documented.[18] After adding an aqueous solution of ICG (6.5 μM, 0.7 mL) into the device, we irradiated the system for 10 min and measured a change in height (Δh_{ICG}) of 33.2 mm. We then derived the μ associated with the σ of a plasmonic nanostructure by first calculating the heat (Q) from Equation (S1). The absorbed irradiation energy (E_{abs}) can be expressed as Equation (S4). Since E_{abs} is completely converted to heat (Q) through Landau damping,[3] we obtain Equation (S6). When the same device is used for both ICG and a suspension of Au nanostructures, the following equation can be used to calculate the μ of the nanostructure (μ_{NS}):

$$\mu_{NS} = -\frac{1}{x}\ln\left[1-\frac{\Delta h_{NS}}{\Delta h_{ICG}}(1-e^{-\mu_{ICG}x})\right] \tag{2}$$

After obtaining μ_{NS} with Equation (2) at the particle concentrations shown in Table 1, we calculated σ using the following equation.[14,19]

$$\sigma = \frac{\mu}{MN_A} \quad (3)$$

where M is the molar concentration of the nanostructures and N_A is the Avogadro constant.

The experimentally obtained μ and σ are listed in Table 1 for each type of Au nanostructure at different concentrations. The magnitude of σ for the nanocages was on the same order as that derived from theoretical calculations (16.3×10^{-15} m^2),[14] suggesting that the PAOF system can be adopted for quantitative measurements of μ and σ. When comparing the σ values of the three different types of Au nanostructures, we found that the nanocages had the highest magnitude, while the nanorods had the lowest magnitude, and the values of σ for both nanorods and hexapods were less than half of that of the nanocages. This finding agrees with the observed tendency for η, in which nanocages exhibited the highest efficiency in converting light to heat. Although prior studies demonstrated that the σ of plasmonic nanostructures could be measured by either photoacoustic imaging[14] or optical coherence tomography,[20] the technique reported in this study provides a much simpler and more convenient method, as it does not require any specific equipment or training.

By taking advantage of the light-driven motion of liquid in a PAOF system, we demonstrated a photo-sensitive electrical switch. In this case, we saturated an aqueous suspension of Au nanocages (1.0×10^{10} particles/mL) with NaCl to make it conductive and then used it as the fluidic medium. We constructed the switch from a small vial connected to a capillary containing two standard copper wires with a gap of 5 mm between their ends (as marked by * and ** symbols in Figure 4a, see also Figure S4 in the Supporting Information). When the solution was irradiated by the diode laser, it heated up and expanded along the capillary, bridging the gap between the two wires and completing an electrical circuit. The connection turned on a small light-emitting diode (LED). After turning off the laser irradiation, the solution level dropped and the LED was switched off. The electrical switch could be operated through four cycles of on and off irradiations without losing its performance (Figure 4b), suggesting that it could be used to control electrical devices without requiring mechanical movement or large solid-state transistors. To our knowledge, this was the first example demonstrating the potential use of fluid motion controlled by plasmonic heating to construct a functional electrical device.

In summary, we have demonstrated a plasmon-assisted optofluidic system by combining the unique features of microfluidics and plasmonic heating of noble-metal nanostructures. By taking advantage of the well-known thermal expansion of a liquid, we could move a fluid column by plasmonic heating. Using this simple system, we were able to quantitatively measure the photothermal conversion efficiencies of various plasmonic nanostructures and their absorption cross sections. We also demonstrated the feasibility of constructing a photo-sensitive, electrical switch by controlling the liquid level with plasmonic heating. Our plasmon-assisted optofluidic system provides a simple and effective platform for remotely controlling the motion of a fluid and is expected to find use in various areas, involving molecular transport, biochemical analysis, catalysis, photonics, and electronics.

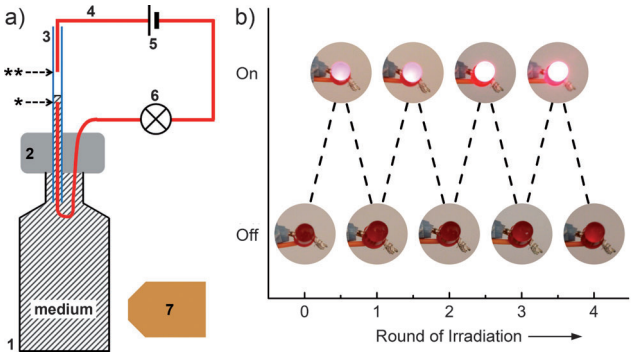

Figure 4. a) Schematic illustration of a photo-responsive electrical switch. A 5 mL glass vial (**1**) was capped with a PDMS block (**2**) inserted with a 1.0 mm capillary tube (**3**). A standard copper wire (**4**) was used to connect the switch to three 1.5 V AA batteries (**5**) connected in series to a standard LED light bulb (**6**). A suspension of Au nanocages (1.0×10^{10} particles/mL) saturated with NaCl was loaded into the vial until it reached the top (*) of the lower copper wire but did not reach the bottom (**) of the upper wire. When the vial was irradiated with a diode laser (**7**), the solution expanded, filling tube **3** and bridging the 5 mm gap between the two copper wires, thus turning on the LED bulb. b) Demonstration of the on–off switching of an LED over four cycles.

Received: December 30, 2012
Published online: March 12, 2013

Keywords: absorption · nanostructures · optofluidics · photothermal conversion · surface plasmon resonance

[1] a) A. O. Govorov, H. H. Richardson, *Nano Today* **2007**, *2*, 30; b) L. R. Hirsch, R. J. Stafford, J. A. Bankson, S. R. Sershen, B. Rivera, R. E. Price, J. D. Hazle, N. J. Halas, J. L. West, *Proc. Natl. Acad. Sci. USA* **2003**, *100*, 13549; c) M. Rycenga, C. M. Cobley, J. Zeng, W. Li, C. H. Moran, Q. Zhang, D. Qin, Y. Xia, *Chem. Rev.* **2011**, *111*, 3669; d) M. Hu, X. Wang, G. V. Hartland, P. Mulvaney, J. P. Juste, J. E. Sader, *J. Am. Chem. Soc.* **2003**, *125*, 14925.

[2] a) S. Link, M. A. El-Sayed, *Annu. Rev. Phy. Chem.* **2003**, *54*, 331; b) W. L. Barnes, A. Dereux, T. W. Ebbesen, *Nature* **2003**, *424*, 824; c) K. L. Kelly, E. Coronado, L. L. Zhao, G. C. Schatz, *J. Phys. Chem. B* **2003**, *107*, 668; d) K. A. Willets, R. P. Van Duyne, *Annu. Rev. Phys. Chem.* **2007**, *58*, 267.

[3] Y. Gao, Z. Yuan, S. Gao, *J. Chem. Phys.* **2011**, *134*, 134702.

[4] a) E. Lukianova-Hleb, Y. Hu, L. Latterini, L. Tarpani, S. Lee, R. A. Drezek, J. H. Hafner, D. O. Lapotko, *ACS Nano* **2010**, *4*, 2109; b) P. K. Jain, I. H. El-Sayed, M. A. El-Sayed, *Nano Today* **2007**, *2*, 18; c) M. T. Carlson, A. J. Green, H. H. Richardson, *Nano Lett.* **2012**, *12*, 1534; d) E. Y. Ye, K. Y. Win, H. R. Tan, M. Lin, C. P. Teng, A. Mlayah, M. Y. Han, *J. Am. Chem. Soc.* **2011**, *133*, 8506.

[5] a) H. Schmidt, A. R. Hawkins, *Nat. Photonics* **2011**, *5*, 598; b) G. Baffou, R. Quidant, F. J. García de Abajo, *ACS Nano* **2010**, *4*, 709; c) T. Ming, L. Zhao, Z. Yang, H. J. Chen, L. D. Sun, J. F. Wang, C. H. Yan, *Nano Lett.* **2009**, *9*, 3896.

[6] a) E. Ozbay, *Science* **2006**, *311*, 189; b) P. Banerjee, D. Conklin, S. Nanayakkara, T.-H. Park, M. J. Therien, D. A. Bonnell, *ACS Nano* **2010**, *4*, 1019.
[7] a) Z. Liu, W. Hou, P. Pavaskar, M. Aykol, S. B. Cronin, *Nano Lett.* **2011**, *11*, 1111; b) J. R. Adleman, D. A. Boyd, D. G. Goodwin, D. Psaltis, *Nano Lett.* **2009**, *9*, 4417; c) P. Christopher, H. Xin, S. Linic, *Nat. Chem.* **2011**, *3*, 41.
[8] a) H. Ma, P. M. Bendix, L. B. Oddershede, *Nano Lett.* **2012**, *12*, 3954; b) G. D. Moon, S.-W. Choi, X. Cai, W. Li, E. C. Cho, U. Jeong, L. V. Wang, Y. Xia, *J. Am. Chem. Soc.* **2011**, *133*, 4762; c) J. Zeng, S. Roberts, Y. Xia, *Chem. Eur. J.* **2010**, *16*, 12559.
[9] a) C. M. Cobley, J. Chen, E. C. Cho, L. V. Wang, Y. Xia, *Chem. Soc. Rev.* **2011**, *40*, 44; b) S. Lal, S. E. Clare, N. J. Halas, *Acc. Chem. Res.* **2009**, *41*, 1842; c) A. G. Skirtach, C. Dejugnat, D. Braun, A. S. Susha, A. L. Rogach, W. J. Parak, H. Mohwald, G. B. Sukhorukov, *Nano Lett.* **2005**, *5*, 1371.
[10] a) D. Erickson, D. Sinton, D. Psaltis, *Nat. Photonics* **2011**, *5*, 583; b) X. Miao, B. K. Wilson, L. Y. Lin, *Appl. Phys. Lett.* **2008**, *92*, 124108; c) X. Fan, I. M. White, *Nat. Photonics* **2011**, *5*, 591; d) J. S. Donner, G. Baffou, D. McCloskey, R. Quidant, *ACS Nano* **2011**, *5*, 5457.
[11] G. L. Liu, J. Kim, Y. Lu, L. P. Lee, *Nat. Mater.* **2006**, 5, 27.
[12] C. Fang, L. Shao, Y. Zhao, J. Wang, H. Wu, *Adv. Mater.* **2012**, *24*, 94.
[13] O. Neumann, A. S. Urban, J. Day, S. Lal, P. Nordlander, N. J. Halas, *ACS Nano* **2013**, DOI: 10.1021/nn304948h.
[14] E. C. Cho, C. Kim, F. Zhou, C. M. Cobley, K. H. Song, J. Chen, Z.-Y. Li, L. V. Wang, Y. Xia, *J. Phys. Chem. C* **2009**, *113*, 9023.
[15] J. Zeng, Q. Zhang, J. Chen, Y. Xia, *Nano Lett.* **2010**, *10*, 30.
[16] a) B. Nikoobakht, M. A. El-Sayed, *Chem. Mater.* **2003**, *15*, 1957; b) T. K. Sau, C. J. Murphy, *Langmuir* **2004**, *20*, 6414.
[17] D. Kim, T. Yu, E. Cho, Y. Ma, O. Park, Y. Xia, *Angew. Chem.* **2011**, *123*, 6452; *Angew. Chem. Int. Ed.* **2011**, *50*, 6328.
[18] Optical Absorption of ICG. http://omlc.ogi.edu/spectra/icg/index.html.
[19] L. V. Wang, H. Wu, *Biomedical Optics: Principles and Imaging*, 1st ed., Wiley, New York, **2007**.
[20] H. Cang, T. Sun, Z.-Y. Li, J. Chen, B. J. Wiley, Y. Xia, X. Li, *Opt. Lett.* **2005**, *30*, 3048.

